Planetary and Space Science 119 (2015) 54–61

Contents lists available at ScienceDirect

Planetary and Space Science

journal homepage: www.elsevier.com/locate/pss

Seasonal variation of Martian pick-up ions: Evidence of breathing exosphere

M. Yamauchi [a,*], T. Hara [b], R. Lundin [c], E. Dubinin [d], A. Fedorov [e], J.-A. Sauvaud [e], R.A. Frahm [f], R. Ramstad [a], Y. Futaana [a], M. Holmstrom [a], S. Barabash [a]

[a] Swedish Institute of Space Physics (IRF), Box 812, SE-98128 Kiruna, Sweden
[b] Space Sciences Laboratory, University of California, Berkeley, CA, USA
[c] Swedish Institute of Space Physics (IRF), Teknikhuset, SE-90187 Umea, Sweden
[d] Max-Planck-Institut fur Sonnensystemforschung, Justus-von-Liebig-Weg 3, DE-37077 Göttingen, Germany
[e] Institut de Recherche en Astrophysique et Planetologie (IRAP), CNRS/Universite de Toulouse, 9 avenue du Colonel Roche, BP 44346, F-31028 Toulouse, Cedex 4 France
[f] Southwest Research Institute, 6220 Culebra Road, San Antonio, TX 78238, USA

ARTICLE INFO

Article history:
Received 16 February 2015
Received in revised form
8 September 2015
Accepted 9 September 2015
Available online 21 September 2015

Keywords:
Pick-up ions
Mars Express
Exosphere
Hydrogen corona
Solar UV effect
Seasonal variation
Solar cycle
Atmospheric escape
ASPERA-3

ABSTRACT

The Mars Express (MEX) Ion Mass Analyser (IMA) found that the detection rate of the ring-like distribution of protons in the solar wind outside of the bow shock to be quite different between Mars orbital summer (around perihelion) and orbital winter (around aphelion) for four Martian years, while the north–south asymmetry is much smaller than the perihelion–aphelion difference. Further analyses using eight years of MEX/IMA solar wind data between 2005 and 2012 has revealed that the detection frequency of the pick-up ions originating from newly ionized exospheric hydrogen with certain flux strongly correlates with the Sun–Mars distance, which changes approximately every two years. Variation due to the solar cycle phase is not distinguishable partly because this effect is masked by the seasonal variation under the MEX capability of plasma measurements. This finding indicates that the variation in solar UV has a major effect on the formation of the pick-up ions, but this is not the only controlling factor.

1. Introduction

Planetary ionospheres and exospheres are affected by the flux from solar extreme ultraviolet (EUV) radiation because the energy required for ionizing atoms or neutrals corresponds to the energy of EUV (Chapman, 1931). As a result, all models of planetary ionospheres and exospheres predict a strong dependency of the ionospheric/exospheric density (at given altitude) on the solar EUV flux (e.g., Lammer et al., 2009; Bougher et al., 2014; Chaufray et al., 2015). For example, the density distribution and behavior of ions above the ionosphere (e.g., escape) are expected to depend on the solar EUV flux.

Observations support the expected dependence of the ionospheric condition and of the resultant ion escape on the solar EUV flux. For the Earth, the ionospheric density changes by an order of magnitude between the solar maximum and minimum in the established International Reference Ionosphere (e.g., Bilitza et al., 2014), and the resulting escape rate of ionospheric oxygen (O^+) is found to vary by more than an order of magnitude between low F10.7 (proxy for EUV flux) and high F10.7 index (Cully et al., 2003). On Venus, the observed ionopause location changes drastically between the solar maximum and minimum, and this change is attributed mainly to the EUV difference (Zhang et al, 1990). The escape rate of the planetary hot ions from the nightside of Mars also depends on the F10.7 flux (Lundin et al., 2013). Lundin et al. (2013) further obtained the escape rate as a simple function of the F10.7 index and the sunspot number.

Planetary ion escape also depends on the extent of the planet's exosphere because the exospheric neutrals that are exposed to the solar wind are lost by a pick-up mechanism (e.g., Luhmann and Kozyra, 1991; Barabash et al., 1991; Dubinin et al., 2006) as soon as they are ionized by the solar EUV, by charge exchange, or by the electron impact ionization. Inversely, refilling of exospheric neutrals that are lost after the ionization causes a faster expansion rate of the exosphere. Therefore, the solar EUV flux strongly influences

* Corresponding author. Tel.: +46 980 79120; fax: +46 980 79050.
E-mail address: M.Yamauchi@irf.se (M. Yamauchi).

http://dx.doi.org/10.1016/j.pss.2015.09.013

the loss rate of the exosphere through both the ionization efficiency and the exospheric scale height.

In such EUV-dependent loss processes, the amount of ionized exospheric neutrals inside the solar wind (including the magnetosheath) is the key number that is important in estimating the total escape of ions of exospheric origin and the dependence of this escape rate on seasonal/solar cycle variations. Among Earth, Venus, and Mars, the role of this mechanism and its seasonal/solar cycle dependence is most dominant at Mars, because the weak gravity of Mars and the large extent of its exosphere beyond the magnetopause or ionopause, causes the exosphere to be exposed to the solar wind.

There are some observations relating how much the Martian exosphere and relevant ion production vary with the solar EUV flux. Using electron data at 390 km altitude from the Mars Global Surveyor (MGS), Forbes et al. (2008) reported nearly two-year variations of the electron density and temperature, and this variation was more evident than the solar cycle variation (see also Bruinsma et al., 2014). Chaffin et al. (2014) used Lyman-alpha emission observed by the Mars Express (MEX) (Chicarro et al, 2004) ultraviolet spectrometer (Bertaux et al., 2006), and showed that the estimated exospheric temperature changed more drastically than the expected change from the EUV variation (see also Chaufray et al., 2009; Clarke et al., 2014). Bertucci et al. (2013) analyzed MGS magnetic field data during one year (from September 1997 to September 1998) and showed that proton cyclotron waves upstream of the bow shock (indication of generation of exospheric-origin cold protons) are observed most frequently during perihelion. However, no direct ion observations have been reported on the solar EUV dependency of the amount of ionized exospheric neutrals in the solar wind.

Mars Express has over 10 years of observations at Mars, including ion mass analyzer (IMA) observations of the solar wind outside the bow shock. In this region, IMA is capable of observing the pick-up ions of exospheric origin (Dubinin et al., 2006; Yamauchi et al., 2006; 2008) as well as reflected solar wind (Yamauchi et al., 2011, 2012). Although there are some operational and observational restrictions in detecting the pick-up ions by IMA, the length and quality of the IMA data are sufficient to statistically diagnose seasonal and solar cycle variations.

2. Instrument

The MEX Analyzer of Space Plasmas and Energetic Atoms (ASPERA-3) experiment contains one ion instrument (IMA), one electron instrument (Electron Spectrometer: ELS), and two instruments to measure energetic neutral atoms.

During more than 10 years of operation, the IMA energy-sweep scheme changed several times to emphasize different regions of the ion energy spectrum (the energy scan from the highest energy to the lowest energy with 12 s cycle was unchanged). Before 30 April 2007, IMA intended to cover a downgoing energy range of 30 keV/q to 10 eV/q with 96 logarithmically scaled energy steps (from about 3 kV to about 1 V potential drop within two spheres of the electrostatic analyzer between which ions travel (Barabash et al., 2004, 2006)), but it turned out that IMA could not accurately determine ions with energies less than 100 eV. Therefore, the IMA energy sweep scheme was reset for the energy range from 30 keV/q to 50 eV/q with 76 logarithmically scaled energy steps and then from 50 eV/q to 10 eV/q in 20 linearly scaled energy steps between 30 April 2007 and 16 November 2009 (Lundin et al., 2009), and from 20 keV to 50 eV/q with 66 logarithmically scaled energy steps and then from 50 eV to −20 eV/q in 30 linearly scaled energy steps after 16 November 2009. This −20 eV/q setting allows IMA to measure ions close to the spacecraft potential and the linear stepping range decreases the rate of voltage decay, allowing the power supply to settle the targeted voltage for an accurate energy measurement.

After completion of the energy scan every 12 s, IMA executes a scan step in elevation. The IMA elevation covers the angular range from −45° to +45° (elevations 0–15) in 192 s using an electrostatic deflection system with about 5° elevation resolution. After 30 April 2007, elevation scanning is disabled on the portion of the energy sweep below 50 eV/q. Since the detection of pick-up ions requires ion measurements at an energy range around the solar wind energy, i.e., from sub-keV to several keV (Yamauchi et al., 2006, 2008; Hara et al., 2013), changes in the energy sweep and elevation scanning do not affect the present study.

IMA also contains a magnetic deflection system (supported by 16 identical permanent magnets) which separates the ions according to M/q after they are electrostatically analyzed. IMA simultaneously measures ions up to 40 amu/q, which spread across a microchannel plate (MCP) sensor depending on the ion energy and M/q, into 32 mass channels. By accelerating ions that went through the energy analyzer before entering the mass analyzer (post acceleration), the mass resolution can be changed between low, medium, and high resolutions (corresponding to high, medium, and no post acceleration, respectively). The low mass-resolution mode is best for detecting the low mass ions like H^+ and He^+, while in the high mass-resolution mode, the solar wind protons are often completely deflected to outside the sensor area. Therefore, one may not mix IMA data taken during different mass-resolution modes for statistical studies. Note that light ions which are deflected outside the sensor area are reflected back from the outer wall of IMA, reaching the sensor in the central area of the MCP, and generating counts in the incorrect mass channels.

MCPs that are used in many medium-energy (around 1 keV) ion sensors including IMA often degrade after long exposure to intense ion beams such as those from the solar wind and radiation belt (e.g., Yamauchi et al., 2013). However, the efficiency of MEX/IMA has not degraded during more than 10 years of operation since the accumulated total count over 10 years was much lower than the specification for the IMA/MCP (In fact, the MCP bias voltage did not require adjusting in order to maintain sensitivity). Therefore, all data collected during 2005–2012 (more than 10000 inbound or outbound traversals across the bow shock) may be treated equally.

ASPERA-3 electrons are measured with Electron Spectrometer (ELS). With angular acceptance width of 4°, ELS covers an energy range from 0.5 eV to 20 keV and is capable of helping identification of bow shock and foreshock, and hence confirming IMA observations of pick-up ions.

Both IMA and ELS are top-hat instruments with 360° azimuthal field of view, divided into 16 sectors (0-15), each 22.5° wide. Note that some reports that have used IMA data refer to different sector numbering (1–16), whereas this paper uses numbering of 0–15 (the same as Yamauchi et al., 2006, 2011). For details of the IMA and ELS instruments, see Barabash et al. (2004, 2006), Fedorov et al. (2006), and Frahm et al. (2006a, 2006b).

3. Analysis methods and restrictions

In the IMA energy–time spectrograms, pick-up ions form a clear ring distribution display (an energy arch) in an energy-azimuth/elevation angle scan at about 2–5 times the solar wind proton energy (Yamauchi et al., 2006, 2008). However, its appearance varies depending on the intensity. Fig. 1 shows three consecutive outbound traversals from the bow shock to upstream solar wind, in which one can recognize the ring-like distribution of pick-up ions at around 3–4 keV in the second traversal (Fig. 1b) as

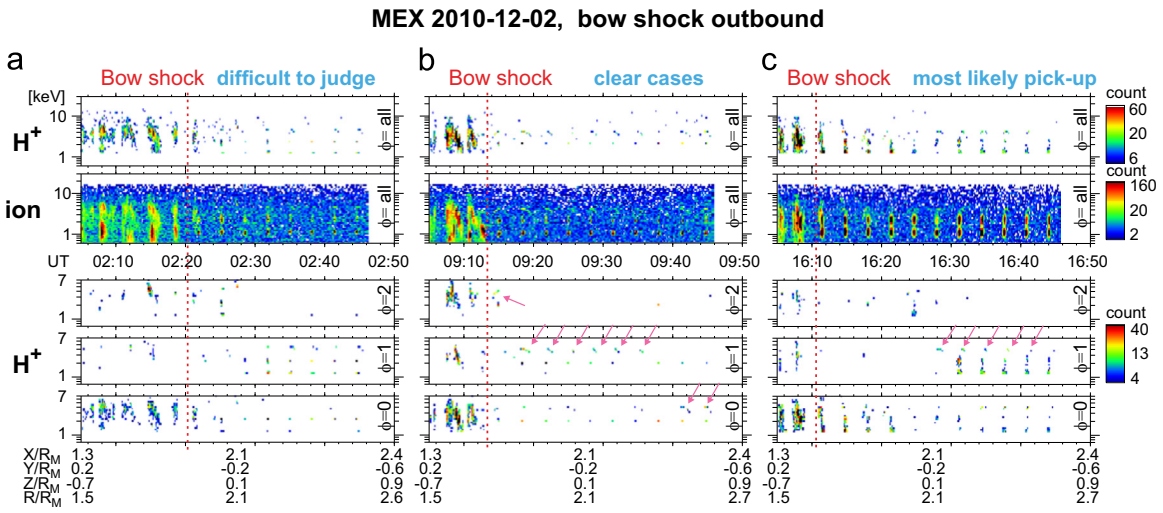

Fig. 1. Examples of ring-like distributions upstream of the bow shock on 2 December 2010 observed by MEX/IMA. Energy–time spectrograms of counts are displayed for the proton channel and total ions at nearly the same location during three consecutive outbound traversals of the bow shock: (a) 02:05–02:50 UT, (b) 09:05–09:50 UT, (c) 16:05–16:50 UT. This is the format and color scale of the spectrogram that was used for the manual (eye-identified) method. The nearly 3-min (192 s) cycle in the IMA data results from scanning in the elevation direction from $-45°$ to $+45°$. Solar wind protons are observed at around 1 keV and alpha particles at around 2 keV. The unit R_M is the Mars radius (3397 km). The middle panels (b) shows the ring-like distribution at around 3–4 keV most clearly. Arrows point to pieces of the ring-like distribution that appear at different azimuths and elevations. (For interpretation of the references to color in this figure legend, the reader is referred to the web version of this article.)

indicated by arrows. The ion distribution at 3–4 keV in the last traversal (Fig. 1c) is not as complete an energy arch as the previous one, but can be recognized as forming partial ring that is consistent with pick-up ions. However, the ion distribution at 3–4 keV in the first traversal (Fig. 1a) does not give a hint of curvature in the spectrogram and therefore it is difficult to judge if these ions are pick-up ions, reflected solar wind, foreshock ions, or even the solar wind O^{6+} (Yamauchi et al., 2011, in press; Nilsson et al., in press).

The change in the intensity during these three consecutive traversals is apparently not due to the change in the IMF orientation. Thus, although MEX is not optimized for studying the pick-up ions (explained in the following paragraph), IMA is capable of judging the appearance and disappearance of the pick-up ions even within a day.

The restrictions in using the IMA data in detecting the pick-up ions are: (a) IMA often misses pick-up ions due to its limited field-of-view (FOV); (b) protons can cleanly be detected only when their energy is above a certain value (above about 1–2 keV depending on the observation mode); (c) temporal resolution is as slow as 192 s (yet MEX/IMA spends sufficient time in the vicinity of the bow shock to obtain adequate spatial resolution as reported in previous studies (Yamauchi et al., 2008, 2011, and 2012)), and (d) the Mars Express payload does not contain a magnetometer (which is necessary to identify the anticipated direction and energy of the ions which gyrate around the local magnetic field direction). As a result, one cannot judge whether the absence of the ring distribution (signature of pick-up ions or reflected ions) is due to a physical process (they are really absent) or an artificial process (partial blockage of the FOV, too low an energy to be efficiently detected, frequent change in the IMF, or a non-optimal orientation of the magnetic field).

Yet, in spite of the above restrictions, the quantity and quality of our dataset (same efficiency for 10 years) allows us to take a statistical approach in obtaining the variation in the occurrence frequency, although the values of probability are only approximate ones, for observing the pick-up ions. The statistical result provides a good diagnosis of the relative variation but not an absolute percentage of observation frequency of the pick-up ions.

Two methods are employed to statistically analyze the ion data: the automated method (Hara et al., 2013) and manual (eye-identified) method (Yamauchi et al., 2006, 2008). The automated method first determines the solar wind velocity. Determination of the solar wind velocity allows prediction of where the ring distribution should appear in velocity space. Every 192 s that covers the entire elevation (from $-45°$ to $+45°$), ion counts above the noise level are examined to determine if they occupy a predicted thin shell in velocity space. If substantial ion counts are found within that shell over several azimuthal–elevation sectors, this observation is determined to be a point (of the total 192 s) that contains the ring distribution. The details of the automated method are explained in Hara et al. (2013).

In the manual method, each traversal inside the solar wind stretching from the bow shock (either inbound or outbound) is counted as a sample with or without the pick-up ion distribution. The criterion used to determine the existence of the pick-up ions (clear cases that corresponds to Fig. 1b) is that the spectrogram in the format of Fig. 1 contain the ring distribution of more than 20 counts/100 ms (in medium mass-resolution mode) over at least four azimuth–elevation sectors with a symmetric elevation-energy pattern (cf. Yamauchi et al., 2006, 2008), and persists over more than three complete elevation scans (i.e. more than about 10 min).

The automated method was used to obtain the difference in the observation probability at the same location between the orbital summer and orbital winter of Mars, where we define Mars' perihelion (hottest point) as orbital summer and its aphelion (coldest point) as orbital winter. Here, we should note that the perihelion (orbital summer) of Mars nearly coincides with the southern summer, and that the perihelion–aphelion difference could also be the summer–winter difference of the southern hemisphere where most of the magnetic anomalies are located (Acuña et al., 1998). On the other hand, the manual method is used (we examined all spectrograms by eye) to obtain the temporal variation of the occurrence of the pick-up ions.

Note that, for the same flux, the proton count rate is completely different between three different mass-resolution modes, and this difference is extremely difficult to calibrate. This results in completely different detection probabilities for the pick-up ions between three mass-resolution modes, as is seen in the difference between Fig. 2a (medium mass resolution mode) and Fig. 2b (lowest mass resolution mode that gives the highest counts for the same flux of the pick-up ions). Unfortunately, IMA was not

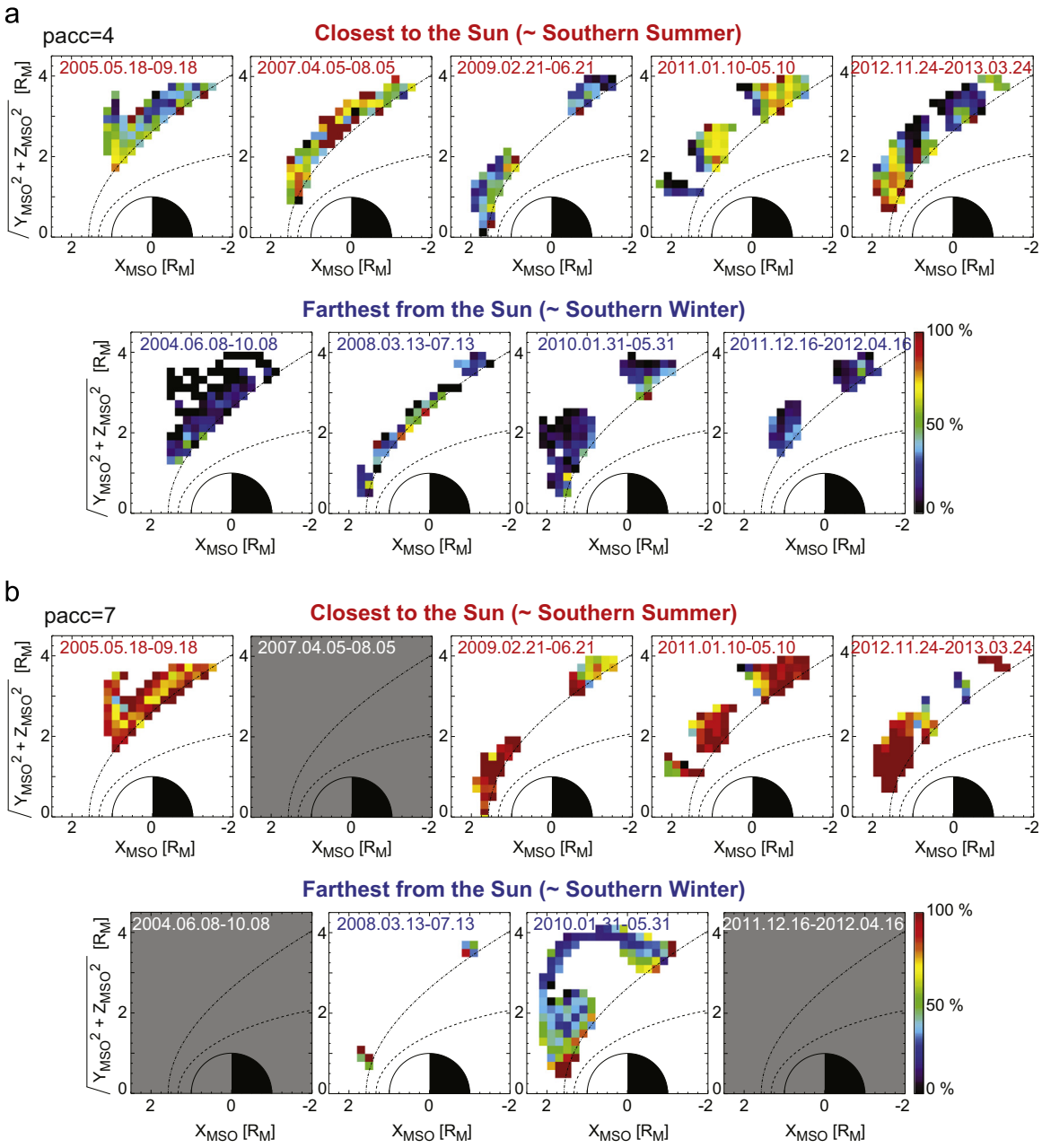

Fig. 2. Probability of observing the ion distribution that is consistent with pick-up ions using the automated method (Hara et al., 2011, 2013), that is applied to dataset from (a) medium mass resolution (pacc=4) mode, and (b) lowest mass resolution (pacc=7) mode. Cylindrical coordinates are used, i.e., vertical axis is distance from the Sun–Mars axis, and the data includes both hemispheres. Probability is calculated over four months during orbital summer (±2 months from perihelion of Mars) and orbital winter (±2 months from aphelion of Mars). Orbital summer and winter defined in this way (by the Sun–Mars distance) correspond closely to summer and winter in the southern hemisphere (the hemisphere with many magnetic anomalies), respectively.

continuously operated under the lowest mass-separation mode, e.g., with sometimes long data gaps. Therefore, the dataset from the medium mass resolution (pacc=4) mode is primarily analyzed for both the automated method and manual method. In addition, the dataset from the lowest mass resolution (pacc=7) mode is also analyzed for the automated method to show the difference between these two modes.

The medium mass-resolution (pacc=4) mode is most frequently used during the entire mission. Yet, there are still data gaps (too little statistics, i.e., less than 20 traversals per 2 months) in 2005, 2006, 2007, and 2011. In our previous studies using the manual method (Yamauchi et al., 2006, 2011, 2012), data from the lowest mass-resolution (pacc=7) were analyzed.

4. Results

Fig. 2 shows the probability of observing the ring-like ion distribution (the pick-up ion occupies a ring that is centered at the solar wind velocity in velocity space) by using the automated method applied to dataset from (a) medium mass resolution (pacc=4) mode and (b) lowest mass resolution (pacc=7) mode.

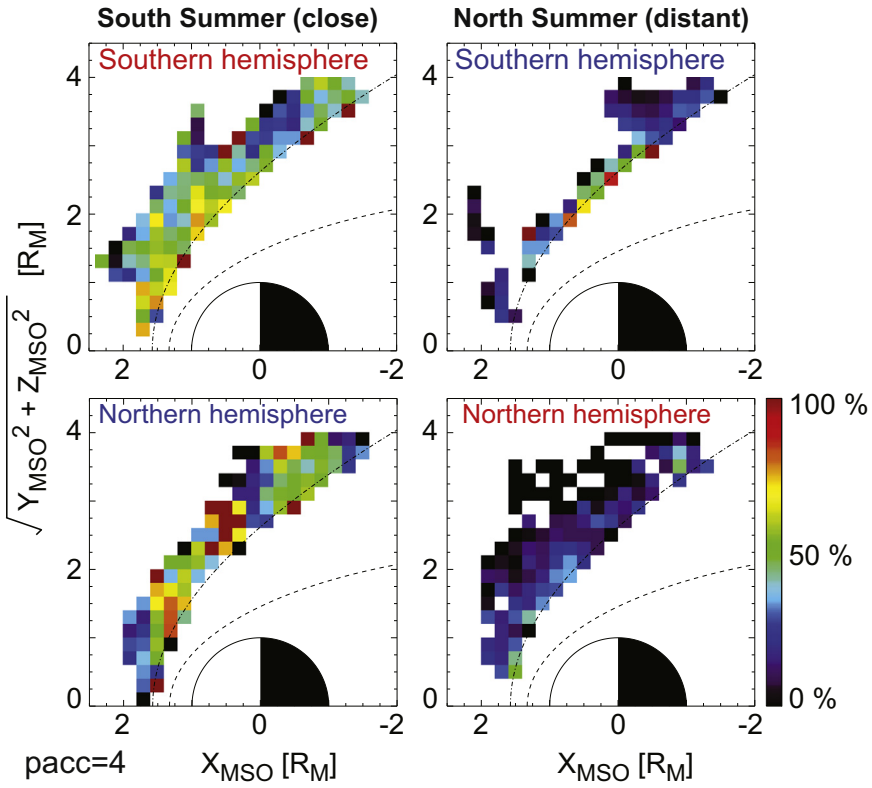

Fig. 3. The same as Fig. 2a except that the MEX traversals of only one hemisphere are used, and that all summer-hemisphere and winter-hemisphere observations are combined.

The data are arranged by the Mars season, i.e., aphelion and perihelion, and presented using the Mars Solar Orbital (MSO) cylindrical coordinate system (i.e., vertical axis of Fig. 2 represents the distance from the Sun–Mars line). As mentioned in the previous section, the lowest mass resolution mode detects the pick-up ions much easier than the medium mass resolution mode, but the number of data is insufficient for statistical studies.

In Fig. 2a, all upper five panels that represent Martian orbital summer months (closest distance to the Sun) show a higher probability of observing the ring-like ion distribution than those for the Martian orbital winter months (farthest distance to the Sun) as shown in the lower four panels. The orbital summer/winter difference is also obvious in Fig. 2b although the statistics are not sufficient. Note that the observed orbital summer–winter difference seen in Fig. 2 might also come from the season of the southern hemisphere as well as the Sun–Mars distance. This question is examined by comparing the summer hemisphere and the winter hemisphere that are defined by the tilt of rotation axis (25° for Mars).

Fig. 3 shows the probability of observing the ring-like distributed ions separated by seasonal hemisphere using data from medium mass resolution (pacc=4) mode. For the orbital summer (around Mars perihelion: left) and orbital winter (around Mars aphelion: right) season, ion distributions in the solar wind are examined for both the southern and northern hemispheres, respectively. Fig. 3 demonstrates that the north–south difference is much smaller than the perihelion–aphelion difference. Thus, the probability depends on the Sun–Mars distance rather than the hemispheric season, and the southern magnetic anomaly field does not affect the generation of pick-up ions (i.e., extent of the hydrogen corona) to detectable extent.

The problem with the automated method is that it cannot distinguish between the pick-up ions and the reflected ions. Within a proton gyroradius (several hundred km) from the bow shock, the reflected solar wind protons are very often detected, and they are sometimes difficult to distinguish from the pick-up ions. The automated method determines a positive selection as long as ions appear at the right place and time, which is independent of the process by which they were created. This is probably the reason why the probability in Fig. 2 is much higher near the empirical bow shock location than the location further away from the bow shock. To compensate for this uncertainly, the probability of observing the pick-up ions was obtained by using the manual (eye-identified) method from the spectrogram.

Fig. 4a shows the result. Red bars represent the detection probability of the "clear" cases like Fig. 1b when the ion distributions satisfy the criterion that is described in the previous section (symmetric elevation-energy pattern, count rate and duration). The ion distributions that do not completely satisfy this condition in intensity (keeping high intensity over 10 min is rather a stringent condition), but are still believed to be of the pick-up ions like Fig. 1c, are displayed with orange bars. Some ring-like ion distributions are difficult to distinguish from reflected ions or foreshock ions like Fig. 1a, or are found only at one 192-s scan, and these difficult cases are marked as gray bars (difficult). We examined all data several times until the eye-identification converged to within a 5% difference between two examinations of the data.

As is shown in Fig. 4a, there are data gaps particularly during a large part of 2006 (observation mode was not appropriate for detecting pick-up ions). In spite of this limitation, Fig. 4a clearly shows the nearly two-year variation that synchronizes with the Sun–Mars distance indicated in Fig. 2. The obvious question then is how well does this change track changes in the EUV flux at Mars.

Fig. 4b shows the estimated solar EUV flux at Mars using the Earth value and Sun–Mars distance. Here, the separation angle between the Earth and Mars is accounted (see the figure caption). Although this method introduces an uncertainty in the estimate of

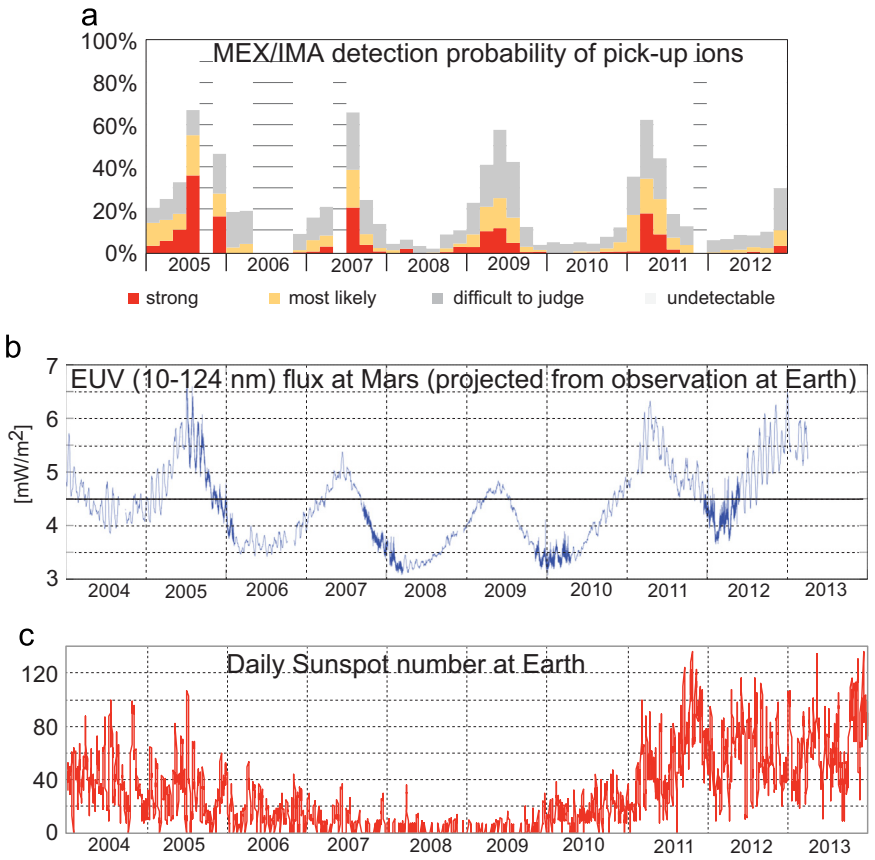

Fig. 4. Temporal variation of (a) observation rate of the pick-up ions determined using the manual method, (b) the estimated EUV flux at Mars from the measured value at the Earth by TIMED/SEE instrument (Woods et al., 1998), and (c) daily sunspot number at the Earth as a proxy for the solar cycle. There are about 7500 solar wind (either inbound or outbound though the bow shock) traversals during 2005–2012 with the medium mass-resolution mode. Note that the total number of hours under a specific mass-resolution mode of IMA varies from time to time, and MEX is sometimes completely downstream of the bow shock for about one month. Therefore, taking monthly averages is not appropriate. However, data becomes rather smooth if two-month time intervals are integrated. Yet, some two-months periods have too few statistics (in 2005, 2006, 2007, and 2011), and two-month periods with less than 25 traversals are not shown. For the EUV flux estimation at Mars, the separation angle between the Earth and Mars is accounted for by time-shifting daily averaged measurements of the TIMES/SEE instrument (Wood et al., 2006) when the angle is more than 45°. For less than 45° of separation, the Earth and Mars are assumed to see approximately the same part of the solar corona, and thus, no time-shifting is applied to observational, time-averaged measurements.

EUV values at Mars, the relative variation of EUV is still well reproduced. In fact, the maximum probability of observing the pick-up ions is found at around the months of highest EUV flux that is regulated by the Sun–Mars distance.

On the other hand, if we take a constant level of EUV flux (e.g., 4.5 mW/m^2 as drawn in Fig. 4b), then the peak probability in 2009 during solar minimum is much higher than the probability in late 2005 or 2012 with higher EUV flux than 2006. Furthermore, the observation probability drastically changes within one season, e.g., from zero percent to more than 15% for clear cases (red bars) and from less than 3% to more than 30% for the most likely cases (orange bars) for both 2007 and 2011, although the EUV flux changes by only 30–40% (due to the variation of the Sun–Mars distance).

5. Summary and discussion

The eight-year data of MEX/IMA during 2005–2012 revealed that the occurrence rate of the pick-up ions varies with Sun–Mars distance, i.e., sharply increases during the Martian orbital summer (around Mars perihelion). The variation thus appears to be mainly driven by the Sun–Mars distance rather than the season of the (southern) hemisphere that possesses large magnetic anomalies. This variation is dominant over the variation at a longer time scale that corresponds to the solar cycle, although MEX/IMA is not capable of judging whether or not the solar cycle effect is seen in the pick-up ion production. Furthermore, the same level of EUV flux, e.g., between the orbital summer of the solar minimum (March–June 2009) and orbital winter of solar maximum (early 2012), results in different probabilities of detection of the pick-up ions.

It should be noted that solid statistics using MEX data are not optimum for conducting plasma measurements of the type required for this study, particularly for the pick up ion distributions. Therefore, Figs. 2–4 give only the variation level of the dominant variation (seasonal effect) but not the absolute percentage of the occurrence rate or variation level of minor variations such as the solar cycle effect. The solid statistics will have to wait until the MAVEN spacecraft is able to obtain sufficient data to produce proper statistics.

Yet, we can state some quantitative outcomes from Fig. 4a. First, in our manual method, the count threshold for clear cases (this is nearly proportional to the energy flux) is about 20 counts per 100 ms observation (cf. the noise level is 2 counts). Therefore, the ion distributions that are classified as "no pick-up ions" have at least one order of magnitude less energy flux (and hence ion density) than the "clear cases". Fig. 4 indicates that gray bars during orbital winter (e.g., 2008 and 2010) show lower values than red bars during orbital summer (mid 2007, mid 2009, and mid 2011), i.e., more than one order of magnitude change in the

pick-up ion flux exists within one season while the solar EUV flux changes only 30–40%.

We are not aware of any model that predicts the order of magnitude change in the density of the hydrogen corona in the solar wind with only 30–40% changes in EUV flux. In other words, this link must be observationally examined by measuring the change in the upper atmospheric density in future. At the present knowledge, the EUV flux seems not the only driver of the observed variation of the pick-up ions, i.e., it is probably not the only factor that controls the total cold ion density originating from the exosphere upstream the bow shock.

The other ionization mechanism that contributes to the cold ion production from the exospheric neutrals upstream the bow shock is charge-exchange, which is proportional to the solar wind flux; however, the perihelion–aphelion variation of the charge-exchange rate is the same level as that of the photo-ionization by the solar EUV. Thus, we need an additional reason to explain the observed orbital variation of the ionization efficiency as shown in Figs. 2 and 4a.

Drastic changes were also observed in the exospheric temperature (Chaffinn et al., 2014) and in the occurrence rate of the proton cyclotron waves (Bertucci et al., 2013), although we have no means to compare the level of orbital (perihelion–aphelion) variation between the present observation and the above observations. It is likely that the EUV is not the only driver of expansion and contraction of the exosphere, i.e., the exosphere might breathe more than what can be accounted for by the EUV alone. One possibility is the effect of the neutral atmosphere due to UV-visible irradiation. Since the Sun–Mars distance also affects the total thermal budget of the Martian atmosphere, such an effect might play a role even on the exospheric expansion. In that case, we might expect a one to two month delay between the Sun–Mars distance and the exospheric expansion due to buffering of the thermal energy in the atmosphere in the same way as the Earth's atmospheric temperature varies.

Second, the time of the peak of the pick-up ion production rate is found to be nearly the same as the perihelion for all orbital summers, but is also consistent with such an atmospheric effect that produces a one to two month of delay from the peak in the UV flux in Fig. 4. By examining the monthly probabilities of pick-up ions, we found peaks in the probabilities for July–August 2007, April–June 2009, and March–May 2011, whereas perihelion occurred June 2007, April 2009, and March 2011. Although this minor shift could be due to instrumental and statistical limitations of the detection of the pick-up ions, a one-month delay is consistent with internal processes of the atmosphere, such as the upper and lower atmospheric temperature (including seasonal variation due to the tilt of the rotation axis) or dust storms (Liemohn et al., 2012). So far, we cannot provide any mechanism for the cause(s) of the overwhelming seasonal variation that does not exactly follow the variation in the EUV flux at both solar cycle scales and few month scales.

Finally, in Fig. 4a, there are few isolated detections of pick-up ions during orbital winter, e.g., during 2008, 2010, and 2012. Quick changes in the intensity of the pick-up ions can occur within one orbit (7 h) as observed in the IMA data presented in the time series in Fig. 1. We are unable to study the reason for such appearances because of the lack of a magnetometer on MEX and limited FOV of IMA. This problem should be solved with full plasma measurements, such as that provided by the MAVEN spacecraft.

Acknowledgment

Both IMA and ELS are part of the ASPERA-3 experiment on the ESA Mars Express spacecraft. We are indebted to all of the involved national agencies and to the European Space Agency for conducting the Mars Express program, especially the Swedish National Space Board, CNRS in France, and NASA (contract NASW-00003) in the USA. EUV values at the Earth is provided by NASA's TIMED/SEE experiment. The sunspot numbers are provided by the Royal Observatory of Belgium, Brussels. The authors thank J. Sharber for valuable comments. The lead author (MY) wishes to thank the social welfare (personal assistant) program in Sweden for providing assistance to physically disabled individuals which made it possible for him to conduct this research.

References

Acuña, M.H., Connerney, J.E.P., Wasilewski, P., Lin, R.P., Anderson, K.A., Carlson, C.W., McFadden, J., Curtis, D.W., Mitchell, D., Reme, H., Mazelle, C., Sauvaud, J.A., D'Uston, C., Cros, A., Medale, J.L., Bauer, S.J., Cloutier, P., Mayhew, M., Winterhalter, D., Ness, N.F., 1998. Magnetic field and plasma observations at Mars: Initial results of the Mars Global Surveyor mission. Science 279 (5357), 1676–1680. http://dx.doi.org/10.1126/science.279.5357.1676.

Barabash, S., Dubinin, E., Pissarenko, N., Lundin, R., Russell, C.T., 1991. Picked-up protons near Mars: Phobos observations. Geophys. Res. Lett. 18, 1805–1808. http://dx.doi.org/10.1029/91GL02082.

Barabash S., Lundin R., Andersson H., Gimholt J., Holmstrom M., Norberg O., Yamauchi M., Asamura K., Coates A.J., Linder D.R., Kataria D.O., Curtis C.C., Hsieh K.C., Sandel B. R., Fedorov A., Grigoriev A., Budnik E., Grande M., Carter M., Reading D.H., Koskinen H., Kallio E., Riihelä P., Säles T., Kozyra J., Krupp N., Livi S., Woch J., Luhmann J., McKenna-Lawlor S., Orsini S., Cerulli-Lrelli R., Maggi M., Morbidini A., Mura A., Milillo A., Roelof E., Williams D., Sauvaud J.-A., Thocaven J.-J., Moreau T., Winningham D., Frahm R., Scherrer J., Sharber J., Wurz P., and Bochsler P., 2004. ASPERA-3: analyser of space plasmas and energetic atoms for Mars Express, in Mars Express: The Scientific Payload, ESA SP-1240, pp. 121–139.

Barabash, S., Lundin, R., Andersson, H., Brinkfeldt, K., Grigoriev, A., Gunell, H., Holmström, M., Yamauchi, M., Asamura, K., Bochsler, P., Wurz, P., Cerulli-Irelli, R., Mura, A., Milillo, A., Maggi, M., Orsini, S., Coates, A.J., Linder, D.R., Kataria, D.O., Curtis, C.C., Hsieh, K.C., Sandel, B.R., Frahm, R.A., Sharber, J.R., Winningham, J.D., Grande, M., Kallio, E., Koskinen, H., Riihelä, P., Schmidt, W., Säles, T., Kozyra, J.U., Krupp, N., Woch, J., Livi, S., Luhmann, J.G., McKenna-Lawlor, S., Roelof, E.C., Williams, D.J., Sauvaud, J.-A., Fedorov, A., Thocaven, J.-J., 2006. The analyzer of space plasmas and energetic atoms (ASPERA-3) for the Mars Express mission. Space Sci. Rev. 126 (1–4), 113–164. http://dx.doi.org/10.1007/s11214-006-9124-8.

Bertaux, J.L., Korablev, O., Perrier, S., Quemerais, E., Montmessin, F., Leblanc, F., Lebonnois, S., Rannou, P., Lefövre, F., Forget, F., Fedorova, A., Dimarellis, E., Reberac, A., Fonteyn, D., Chaufray, J.Y., Guibert, S., 2006. SPICAM on Mars Express: observing modes and overview of UV spectrometer data and scientific results. J. Geophys. Res. 111, E10S90. http://dx.doi.org/10.1029/2006JE002690.

Bertucci, C., Romanelli, N., Chaufray, J.Y., Gomez, D., Mazelle, C., Delva, M., Modolo, R., Gonzalez-Galindo, F., Brain, D.A., 2013. Temporal variability of waves at the proton cyclotron frequency upstream from Mars: implications for Mars distant hydrogen exosphere. Geophys. Res. Lett. 40 (15), 3809–3813. http://dx.doi.org/10.1002/grl.50709.

Bilitza, D., Altadill, D., Zhang, Y., Mertens, C., Truhlik, V., Richards, P., McKinnell, L.-A., Reinisch, B., 2014. The International Reference Ionosphere 2012 – a model of international collaboration. J. Space Weather Space Clim. 4, A07. http://dx.doi.org/10.1051/swsc/2014004.

Bougher, S.W., Cravens, T.E., Grebowsky, J., Luhmann, J., 2014. The aeronomy of Mars: characterization by MAVEN of the upper atmosphere reservoir that regulates volatile escape. Space Sci. Rev. . http://dx.doi.org/10.1007/s11214-014-0053-7, online

Bruinsma, S., Forbes, J.M., Marty, J.C., Zhang, X., Smith, M.D., 2014. Long‚Äêterm variability of Mars' exosphere based on precise orbital analysis of Mars Global Surveyor and Mars Odyssey. J. Geophys. Res. 119 (1), 210–218. http://dx.doi.org/10.1002/2013JE004491.

Chaffin, M.S., Chaufray, J.Y., Stewart, I., Montmessin, F., Schneider, N.M., Bertaux, J.L., 2014. Unexpected variability of Martian hydrogen escape. Geophys. Res. Lett. 41 (2), 314–320. http://dx.doi.org/10.1002/2013GL058578.

Chapman, S., 1931. The absorption and dissociation or ionizing effect of monochromatic radiation in an atmosphere on a rotating Earth. Proc. Phys. Soc. Lond. 43, 26–45. http://dx.doi.org/10.1088/0959-5309/43/1/305.

Chaufray, J.-Y., Leblanc, F., Quemerais, E., Bertaux, J.L., 2009. Martian oxygen density at the exobase deduced from O I 130.4-nm observations by spectroscopy for the investigation of the characteristics of the atmosphere of Mars on Mars Express. J. Geophys. Res. 114, E02006. http://dx.doi.org/10.1029/2008JE003130.

Chaufray, J.-Y., Gonzalez-Galindo, F., Forget, F., Lopez-Valverde, M.A., Leblanc, F., Modolo, R., Hess, S., 2015. Variability of the hydrogen in the Martian upper atmosphere as simulated by a 3D atmosphere-exosphere coupling. Icarus 245, 282–294. http://dx.doi.org/10.1016/j.icarus.2014.08.038.

Chicarro, A., Martin, P., Trautner, R., 2004. The Mars Express mission: An overview, in MARS EXPRESS: The Scientific Payload. In: Wilson, A. (Ed.), European Space Agency Publications Division. European Space Research & Technology Centre, Noordwijk, The Netherlands, pp. 3–13, ESA SP-1240.

Clarke, J.T., Bertaux, J.L., Chaufray, J.Y., Gladstone, G.R., Quemerais, E., Wilson, J.K., Bhattacharyya, D., 2014. A rapid decrease of the hydrogen corona of Mars. Geophys. Res. Lett. 41 (22), 8013–8020. http://dx.doi.org/10.1002/2014GL061803.

Cully, C.M., Donovan, E.F., Yau, A.W., Arkos, G.G., 2003. Akebono/suprathermal mass spectrometer observations of low energy ion outflow: dependence on magnetic activity and solar wind conditions. J. Geophys. Res. 108 (A2), 1093. http://dx.doi.org/10.1029/2001JA009200.

Dubinin, E., Fraenz, M., Woch, J., Barabash, S., Lundin, R., Yamauchi, M., 2006. Hydrogen exosphere at Mars: Pickup protons and their acceleration at the bow shock. Geophys. Res. Lett. 33, L22103. http://dx.doi.org/10.1029/2006GL027799.

Fedorov, A., Budnik, E., Sauvaud, J.-A., Mazelle, C., Barabash, S., Lundin, R., Acuna, M., Holström, M., Grigoriev, A., Yamauchi, M., Andersson, H., Thocaven, J.J., Winningham, D., Frahm, R., Sharber, J.R., Scherrer, J., Coates, A.J., Linder, D.R., Kataria, D.O., Kallio, E., Koskinen, H., Säles, T., Riihelä, P., Schmidt, W., Kozyra, J., Luhmann, J., Roelof, E., Williams, D., Livi, S., Curtis, C.C., Hsieh, K.C., Sandel, B.R., Grande, M., Carter, M., McKenna-Lawler, S., Orsini, S., Cerulli-Irelli, R., Maggi, M., Wurz, P., Bochsler, P., Krupp, N., Woch, J., Fränz, M., Asamura, K., Dierker, C., 2006. Structure of the Martian wake. Icarus 182 (2), 329–336. http://dx.doi.org/10.1016/j.icarus.2005.09.021.

Forbes, J.M., Lemoine, F.G., Bruinsma, S.L., Smith, M.D., Zhang, X., 2008. Solar flux variability of Mars: exosphere densities and temperatures. Geophys. Res. Lett. 35, L01201. http://dx.doi.org/10.1029/2007GL031904.

Frahm, R.A., Winningham, J.D., Sharber, J.R., Scherrer, J.R., Jeffers, S.J., Coates, A.J., Linder, D.R., Kataria, D.O., Lundin, R., Barabash, S., Holmström, M., Andersson, H., Yamauchi, M., Grigoriev, A., Kallio, E., Säles, T., Riihelä, P., Schmidt, W., Koskinen, H., Kozyra, J.U., Luhmann, J.G., Roelof, E.C., Williams, D.J., Livi, S., Curtis, C.C., Hsieh, K.C., Sandel, B.R., Grande, M., Carter, M., Sauvaud, J.-A., Fedorov, A., Thocaven, J.-J., McKenna-Lawler, S., Orsini, S., Cerulli-Irelli, R., Maggi, M., Wurz, P., Bochsler, P., Krupp, N., Woch, J., Fränz, M., Asamura, K., Dierker, C., 2006a. Carbon dioxide photoelectron energy peaks at Mars. Icarus 182 (2), 371–382. http://dx.doi.org/10.1016/j.icarus.2006.01.014.

Frahm, R.A., Sharber, J.R., Winningham, J.D., Wurz, P., Liemohn, M.W., Kallio, E., Yamauchi, M., Lundin, R., Barabash, S., Coates, A.J., Linder, D.R., Kozyra, J.U., Holmström, M., Jeffers, S.J., Andersson, H., McKenna-Lawler, S., 2006b. Locations of atmospheric photoelectron energy peaks within the Mars environment. Space Sci. Rev. 126, 389–402. http://dx.doi.org/10.1007/s11214-006-9119-5.

Hara, T., Seki, K., Futaana, Y., Yamauchi, M., Yagi, M., Matsumoto, Y., Tokumaru, M., Fedorov, A., Barabash, S., 2011. Heavy-ion flux enhancement in the vicinity of the Martian ionosphere during CIR passage: Mars Express ASPERA-3 observations. J. Geophys. Res. 116, A02309. http://dx.doi.org/10.1029/2010JA015778.

Hara, T., Seki, K., Futaana, Y., Yamauchi, M., Barabash, S., Fedorov, A.O., Yagi, M., Delcourt, D.C., 2013. Statistical properties of planetary heavy-ion precipitations toward the Martian ionosphere obtained from Mars Express. J. Geophys. Res. Space Phys. 118, 5348–5357. http://dx.doi.org/10.1002/jgra.50494.

Lammer, H., Bredehöft, J.H., Coustenis, A., Khodachenko, M.L., Kaltenegger, L., Grasset, O., Prieur, D., Raulin, F., Ehrenfreund, P., Yamauchi, M., Wahlund, J.-E., Griessmeier, J.-M., Stangl, G., Cockell, C.S., Kulikov, Yu.N., Grenfell, J.-L., Rauer, H., 2009. What makes a planet habitable? Astron. Astrophys. Rev. 17, 181–249. http://dx.doi.org/10.1007/s00159-009-0019-z.

Liemohn, M.W., Dupre, A., Bougher, S.W., Trantham, M., Mitchell, D.L., Smith, M.D., 2012. Time-history influence of global dust storms on the upper atmosphere at Mars. Geophys. Res. Lett. 39, L11201. http://dx.doi.org/10.1029/2012GL051994.

Luhmann, J.G., Kozyra, J.U., 1991. Dayside pickup oxygen ion precipitation at Venus and Mars: spatial distributions, energy deposition and consequences. J. Geophys. Res. 96 (A4), 5457–5467. http://dx.doi.org/10.1029/90JA01753.

Lundin, R., Barabash, S., Holmström, M., Nilsson, H., Yamauchi, M., Dubinin, E.M., Fraenz, M., 2009. Atmospheric origin of cold ion escape from Mars. Geophys. Res. Lett. 36, L17202. http://dx.doi.org/10.1029/2009GL039341.

Lundin, R., Barabash, S., Holmström, M., Nilsson, H., Futaana, Y., Ramstad, R., Yamauchi, M., Dubinin, E., Fraenz, M., 2013. Solar cycle effects on the ion escape from Mars. Geophys. Res. Lett. 40 (23), 6028–6032. http://dx.doi.org/10.1002/2013GL058154.

Nilsson, H., Wieser, G.S., Behar, E., Wedlund, C.S., Kallio, E., Gunell, H., Edberg, N., Eriksson, A.I., Yamauchi, M., Koenders, C., Wieser, M., Lundin, R., Barabash, S., Mandt, K., Burch, J.L., Goldstein, R., Mokashi, P., Carr, C., Cupido, E., Fox, P.T., Szego, K., Nemeth, Z., Fedorov, A., Sauvaud, J.-A., Koskinen, H., Richter, I., Lebreton, J.-P., Henri, P., Volwerk, M., Vallat, C., Geiger, B., 2015. Evolution of the ion environment of comet 67P/Churyumov-Gerasimenko. Astron. Astrophys. . http://dx.doi.org/10.1051/0004-6361/201526142, in press

Woods, T.N., Eparvier, F.G., Bailey, S.M., Solomon, S.C., Rottman, G.J., Lawrence, G.M., Roble, R.G., White, O.R., Lean, J., Tobiska, W.K., 1998. TIMED Solar EUV Experiment, in Missions to the Sun II. SPIE Proc. 3442, 180–191. http://dx.doi.org/10.1117/12.330255.

Yamauchi, M., Futaana, Y., Fedorov, A., Dubinin, E., Lundin, R., Sauvaud, J.-A., Winningham, D., Frahm, R., Barabash, S., Holmström, M., Woch, J., Fraenz, M., Budnik, E., Borg, H., Sharber, J.R., Coates, A.J., Soobiah, Y., Koskinen, H., Kallio, E., Asamura, K., Hayakawa, H., Curtis, C., Hsieh, K.C., Sandel, B.R., Grande, M., Grigoriev, A., Wurz, P., Orsini, S., Brandt, P., McKenna-Lawler, S., Kozyra, J., Luhmann, J., 2006. IMF direction derivation from cycloid-like ion distributions observed by Mars Express. Space Sci. Rev. 126 (1–4), 239–266. http://dx.doi.org/10.1007/s11214-006-9090-1.

Yamauchi, M., Futaana, Y., Fedorov, A., Kallio, E., Frahm, R.A., Lundin, R., Sauvaud, J.-A., Winningham, D.J., Barabash, S., Holmström, M., 2008. Advanced method to derive the IMF direction near Mars from cycloidal proton distributions. Planet. Space Sci. 56 (8), 1145–1154. http://dx.doi.org/10.1016/j.pss.2008.02.012.

Yamauchi, M., Futaana, Y., Fedorov, A., Frahm, R.A., Winningham, J.D., Dubinin, E., Lundin, R., Barabash, S., Holmström, M., Mazelle, C., Sauvaud, J.-A., Zhang, T.L., Baumjohann, W., Coates, A.J., Fraenz, M., 2011. Comparison of accelerated ion populations observed upstream of the bow shocks at Venus and Mars. Ann. Geophys. 29 (3), 511–528. http://dx.doi.org/10.5194/angeo-29-511-2011.

Yamauchi, M., Futaana, Y., Fedorov, A., Frahm, R.A., Dubinin, E., Lundin, R., Sauvaud, J.-A., Winningham, J.D., Barabash, S., Holmström, M., 2012. Ion acceleration by multiple reflections at Martian bow shock. Earth Planets Space 64 (2), 61–71. http://dx.doi.org/10.5047/eps.2011.07.007.

Yamauchi, M., Dandouras, I., Reme, H., Lundin, R., Kistler, L.M., 2013. Cluster observation of few-hour-scale evolution of structured plasma in the inner magnetosphere. Ann. Geophys., 31, 1569–1578. http://dx.doi.org/10.5194/angeo-31-1569-2013.

Yamauchi, M., Lundin, R., Frahm, R.A., Sauvaud, J.-A., Holmström, M., Barabash, S., 2015. Oxygen foreshock of Mars. Planet. Space Sci. http://dx.doi.org/10.1016/j.pss.2015.08.003.

Zhang, T.L., Luhmann, J., Russell, C.T., 1990. The solar cycle dependence of the location and shape of the Venus bow shock. J. Geophys. Res. 95 (A9), 14961–14967. http://dx.doi.org/10.1029/JA095iA09p14961.